Electronic Supplementary Material (ESI) for Reaction Chemistry & Engineering.

Supporting Information

for

Alternate pathway for standard SCR on Cu-Zeolites with gas-phase ammonia

Rohil Daya[1]*, Christopher J. Keturakis[2], Dylan Trandal[1], Ashok Kumar[1], Saurabh Y. Joshi[1], Aleksey Yezerets[1]

[1]*Cummins Inc., 1900 McKinley Ave, Columbus, IN 47201, U.S.A.*

[2]*Cummins Emission Solutions, 1801 US Highway 51/138, Stoughton, WI 53589, U.S.A*

E-mail : rohil.daya@cummins.com

1. Reaction Mechanism for Site-Specific SCR Model

The site-specific model utilized here builds upon our previous work on a 3-site NH_3 storage model to simulate NH_3 TPD (temperature programmed desorption) as a function of hydrothermal aging [1]. The model structure on Brønsted acid sites and Physisorbed sites is retained with similar rate parameters, while the lumped Copper sites are separated into Z_2Cu and ZCuOH sites. Number densities of Z_2Cu and ZCuOH sites are estimated through NO_2-TPD and NO + NH_3 titration experiments, as reported in [2].

We consider up to 1 NH_3 adsorbed per ZCuOH site, and up to 2 NH_3 to adsorb per Z_2Cu site, consistent with previous quantification of NH_3 adsorbed per Cu site at 200°C in 10% O_2 and 7% H_2O [1, 3]. While DFT calculations and spectroscopic investigations suggest NH_3/Cu ratios of 4 for Z_2Cu sites, and 3 for ZCuOH sites [4-5], this level of NH_3 solvation is likely achieved at temperatures below 200°C. The additional NH_3 adsorption on Cu sites at low temperatures is lumped into the Physisorbed site, which also includes weakly bound NH_3 on Brønsted acid sites and Lewis acidic extra-framework aluminum sites. The desorption activation energies on isolated Cu sites are consistent with DFT estimations in [4]. More details on the identification of adsorption-desorption kinetics and surface coverages on each site are included in [1, 6].

Standard SCR is assumed to occur through the reaction of NO with NH_3-solvated Cu species, consistent with the current state of understanding [7-8]. This is represented globally in the model through reactions R7 and R8 (Table S1). Rate parameters for these SCR reactions are estimated using kinetic regime experimental data on catalysts with different proportions of Z_2Cu and ZCuOH sites. More details on this will be included in a future publication. The overall reaction mechanism is shown in Table S1.

Table S1

Site-Specific NH_3 Storage and Standard SCR Reaction Mechanism on Cu-SSZ-13

Reaction Number	Reaction	Rate Expression
R1	$NH_3 + ZH \leftrightarrow ZNH_4$	$r_{Ads_{ZH}} = k_{Ads_{ZH}} y_{NH_3,s} \theta_{ZH} \Omega_{ZH}$ $r_{Des_{ZH}} = k_{Des_{ZH}} \theta_{ZNH_4} \Omega_{ZH}$
R2	$NH_3 + ZNH_4 \leftrightarrow ZNH_4NH_3$	$r_{Ads_{ZNH_4}} = k_{Ads_{ZNH_4}} y_{NH_3,s} \theta_{ZNH_4} \Omega_{ZH}$ $r_{Des_{ZNH_4}} = k_{Des_{ZNH_4}} \theta_{ZNH_4NH_3} \Omega_{ZH}$
R3	$NH_3 + P \leftrightarrow PNH_3$	$r_{Ads_P} = k_{Ads_P} y_{NH_3,s} \theta_P \Omega_P$ $r_{Des_P} = k_{Des_P} \theta_{PNH_3} \Omega_P$
R4	$NH_3 + ZCuOH \leftrightarrow ZCuOHNH_3$	$r_{Ads_{ZCuOH}} = k_{Ads_{ZCuOH}} y_{NH_3,s} \theta_{ZCuOH} \Omega_{ZCuOH}$ $r_{Des_{ZCuOH}} = k_{Des_{ZCuOH}} \theta_{ZCuOHNH_3} \Omega_{ZCuOH}$

R5	$NH_3 + Z_2Cu \leftrightarrow Z_2CuNH_3$	$r_{Ads_{Z_2Cu}} = k_{Ads_{Z_2Cu}} y_{NH_3,s} \theta_{Z_2Cu} \Omega_{Z_2Cu}$ $r_{Des_{Z_2Cu}} = k_{Des_{Z_2Cu}} \theta_{Z_2CuNH_3} \Omega_{Z_2Cu}$
R6	$NH_3 + Z_2CuNH_3 \leftrightarrow Z_2Cu(NH_3)_2$	$r_{Ads_{Z_2CuNH_3}} = k_{Ads_{Z_2CuNH_3}} y_{NH_3,s} \theta_{Z_2CuNH_3} \Omega_{Z_2Cu}$ $r_{Des_{Z_2CuNH_3}} = k_{Des_{Z_2CuNH_3}} \theta_{Z_2Cu(NH_3)_2} \Omega_{Z_2Cu}$
R7	$4ZCuOHNH_3 + 4NO + O_2 \rightarrow 4ZCuOH + 4N_2 + 6H_2O$	$r_{SSCR_{ZCuOH}} = k_{SSCR_{ZCuOH}} y_{NO,s}^{0.8} y_{O_2}^{0.3} \theta_{ZCuOHNH_3} \Omega_{ZCuOH}$
R8	$2Z_2Cu(NH_3)_2 + 4NO + O_2 \rightarrow 2Z_2Cu + 4N_2 + 6H_2O$	$r_{SSCR_{Z_2Cu}} = k_{SSCR_{Z_2Cu}} y_{NO,s}^{0.8} y_{O_2}^{0.3} \theta_{Z_2Cu(NH_3)_2} \Omega_{Z_2Cu}$

2. Dynamic NO_x Conversion as a function of Temperature and NO Feed

Figure S1 shows the initial change in the NO_x conversion vs. NH_3 storage for 200 ppm and 1000 ppm feed NO from 175°C-250°C. The contribution of the initial increase in NO_x conversion to the overall steady-state conversion appears to increase with increasing feed and decreasing temperatures

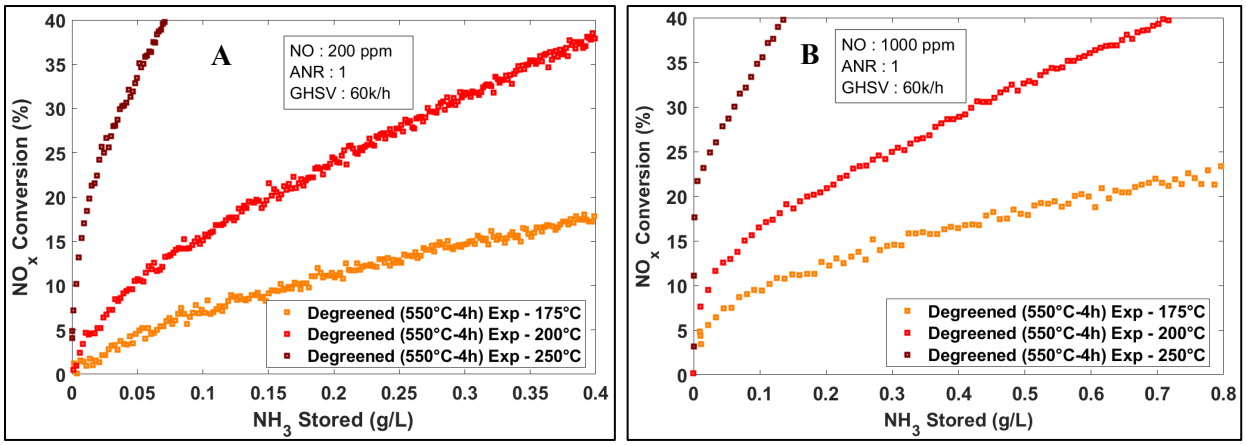

Figure S1. Initial NO_x Conversion as a function of NH_3 storage and catalyst temperature under standard SCR conditions ($NO_2/NO_x = 0$) at 60k/h GHSV and ANR 1 with **A.** Feed NO : 200 ppm and **B.** Feed NO : 1000 ppm

3. Site-Specific Model for Reduction of Cu^{2+} Sites

3.1 Reaction Mechanism

To model the reduction half cycle of the standard SCR reaction, we utilized the same NH_3 storage model framework shown in Table S1. We included the interaction of NO with NH_3 solvated Cu sites to generate reduced Cu sites, and the subsequent NH_3 solvation of the reduced Cu sites. Activation energies for the reduction of ZCuOH and Z_2Cu sites were set to 71 kJ/mol and 74 kJ/mol respectively, as reported from

theoretical calculations in [4]. Reaction pre-exponentials are estimated from NO + NH_3 titration experiments on catalysts with different proportions of Z_2Cu and ZCuOH sites. More details on this will be included in a future publication. Following the reduction of Cu sites and subsequent NH_3 solvation, a temperature programmed desorption (TPD) experiment was run to desorb the NH_3 from reduced Cu and Bronsted acid sites (similar protocol to NH_3-TPD on oxidized catalysts). This information was utilized to estimate the adsorption-desorption kinetics for the reduced Cu sites. More details on the identification of these kinetics and surface coverages on each site are included in [6]. The overall reaction mechanism is shown in Table S2.

Table S2

Reaction Mechanism for Reduction of ZCuOH and Z_2Cu Sites on Cu-SSZ-13

Reaction Number	Reaction	Rate Expression
R7	$ZCuOHNH_3 + NO \rightarrow ZCu + N_2 + 2H_2O$	$r_{RHC_{ZCuOH}} = k_{RHC_{ZCuOH}} y_{NO,s} \theta_{ZCuOHNH_3} \Omega_{ZCuOH}$
R8	$Z_2CuNH_3 + NO \rightarrow ZCu + ZH + N_2 + H_2O$	$r_{RHC_{Z_2Cu}} = k_{RHC_{Z_2Cu}} y_{NO,s} \theta_{Z_2CuNH_3} \Omega_{Z_2Cu}$
R9	$Z_2Cu(NH_3)_2 + NO \rightarrow ZCuNH_3 + ZH + N_2 + 2H_2O$	$r_{RHC2_{Z_2Cu}} = k_{RHC2_{Z_2Cu}} y_{NO,s} \theta_{Z_2Cu(NH_3)_2} \Omega_{Z_2Cu}$
R10	$NH_3 + ZCu \leftrightarrow ZCuNH_3$	$r_{Ads_{ZCu}} = k_{Ads_{ZCu}} y_{NH_3,s} \theta_{ZCu} \Omega_{ZCu}$ $r_{Des_{ZCu}} = k_{Des_{ZCu}} \theta_{ZCuNH_3} \Omega_{ZCu}$
R11	$NH_3 + ZCuNH_3 \leftrightarrow ZCu(NH_3)_2$	$r_{Ads_{ZCuNH_3}} = k_{Ads_{ZCuNH_3}} y_{NH_3,s} \theta_{ZCuNH_3} \Omega_{ZCu}$ $r_{Des_{ZCuNH_3}} = k_{Des_{ZCuNH_3}} \theta_{ZCu(NH_3)_2} \Omega_{ZCu}$

3.2 Results

Figure S2 compares the NO consumption experimental data against the model predictions. While the model reasonably predicts the overall qualitative NO consumption rates, the initial NO consumption is significantly underpredicted. This is associated with the requirement for NH_3 solvation of Z_2Cu and ZCuOH sites prior to reduction, inconsistent with observed experimental data.

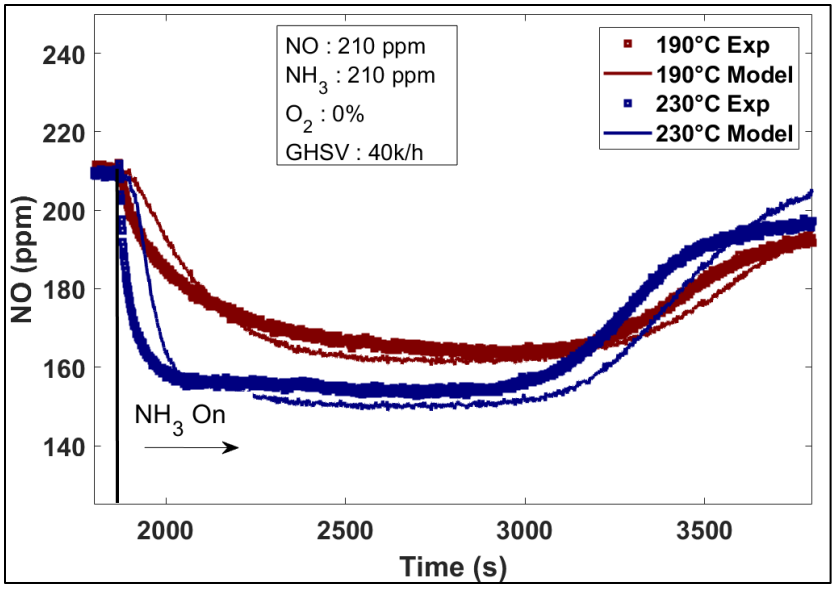

Figure S2. NO Consumption during NO + NH_3 titration of Cu^{2+} sites. Squares represent experimental data and lines represents model results (190°C in dark red, 230°C in dark blue)

4. Influence of SCR reaction with gas-phase NH_3 on Dynamic NO_x Conversion at 200°C and 175°C

Figure S3 plots the complete dynamic NO_x conversion curve at 200°C and 175°C, comparing the two kinetic models with experimental data. The influence of the SCR reaction with gas-phase NH_3 is primarily observed at low NH_3 coverage and the addition of this reaction in the kinetic model leads to accurate representation of the experimental data.

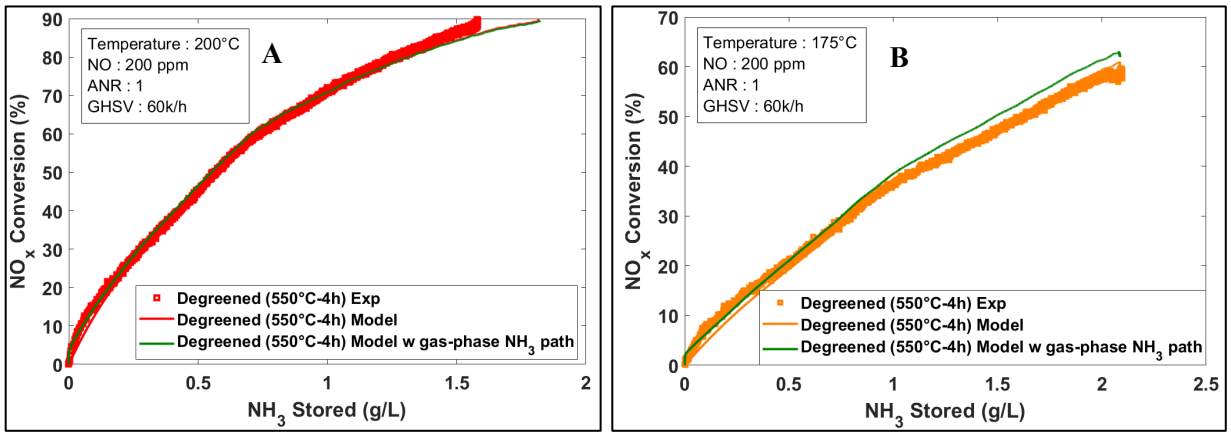

Figure S3. NO_x Conversion as a function of NH_3 storage under standard SCR conditions at **A.** 200°C and **B.** 175°C. Squares represent experimental data and lines represent model results

5. Standard SCR Reaction Order in NH_3

5.1 Analytical Expression

In general, the NH_3 reaction order for standard SCR can be estimated as:

$$o_{NH_3} = y_{NH_3,s}\frac{\partial \ln(r_{sscr})}{\partial y_{NH_3,s}} \tag{1}$$

Utilizing the rate expressions for standard SCR with adsorbed-NH_3 and gas-phase NH_3 (Table 1 in main manuscript), we can write the overall SCR rate as:

$$r_{sscr} = k_{sscr1}y_{NO,s}y_{O_2}^{0.32}\theta_{NH_3S1}\Omega_1 + \frac{k_{sscr2}y_{NO}y_{O_2}^{0.32}y_{NH_3,s}\Omega_1}{1+K_{inh}y_{NH_3,s}} \tag{2}$$

The definition of steady state can be used to express the NH_3 surface coverage as a function of the NO and NH_3 surface mole fractions, as shown in equation (4).

$$\frac{\partial \theta_{NH_3S1}}{\partial t} = k_{Ads}y_{NH_3,s}(1-\theta_{NH_3S1}) - (k_{Des1}+k_{Des2})\theta_{NH_3S1} - k_{sscr1}y_{NO,s}y_{O_2}^{0.32}\theta_{NH_3S1} = 0 \tag{3}$$

$$\Rightarrow \quad \theta_{NH_3S1} = \frac{k_{Ads}y_{NH_3,s}}{k_{Ads}y_{NH_3,s}+(k_{Des1}+k_{Des2})+k_{sscr1}y_{NO,s}y_{O_2}^{0.32}} \tag{4}$$

Using the result from equation (4) in equation (2) , we have:

$$r_{sscr} = \frac{k_{sscr1}y_{NO,s}y_{O_2}^{0.32}k_{Ads}y_{NH_3,s}\Omega_1}{k_{Ads}y_{NH_3,s}+(k_{Des1}+k_{Des2})+k_{sscr1}y_{NO,s}y_{O_2}^{0.32}} + \frac{k_{sscr2}y_{NO}y_{O_2}^{0.32}y_{NH_3,s}\Omega_1}{1+K_{inh}y_{NH_3,s}} \tag{5}$$

Multiplying both sides of equation (5) by the natural logarithm, we obtain the following result:

$$\begin{aligned}\ln r_{sscr} = {} & \ln\left(k_{sscr1}y_{O_2}^{0.32}\Omega_1\right) + \ln y_{NO,s} + \ln\left(k_{Ads}y_{NH_3,s}\right) - \ln\left(k_{Ads}y_{NH_3,s} + (k_{Des1}+k_{Des2}) + \right.\\ & \left. k_{sscr1}y_{NO,s}y_{O_2}^{0.32}\right) + \ln\left(k_{sscr2}y_{O_2}^{0.32}\Omega_1\right) + \ln y_{NO,s} + \ln y_{NH_3,s} - \ln(1+K_{inh}y_{NH_3,s})\end{aligned} \tag{6}$$

Differentiating equation (6) in $y_{NH_3,s}$ and using the result in equation (1) leads to the following expression for NH_3 reaction order

$$\begin{aligned}o_{NH_3} = y_{NH_3,s}\frac{\partial \ln(r_{sscr})}{\partial y_{NH_3,s}} = {} & y_{NH_3,s}\left(\frac{1}{y_{NO,s}}\frac{\partial y_{NO,s}}{\partial y_{NH_3,s}} + \frac{1}{y_{NH_3,s}} - \frac{k_{Ads}+\frac{\partial(k_{Des1}+k_{Des2})}{\partial y_{NH_3,s}} + k_{sscr1}y_{O_2}^{0.32}\frac{\partial y_{NO,s}}{\partial y_{NH_3,s}}}{k_{Ads}y_{NH_3,s}+(k_{Des1}+k_{Des2})+k_{sscr1}y_{NO,s}y_{O_2}^{0.32}} + \right.\\ & \left. \frac{1}{y_{NO,s}}\frac{\partial y_{NO,s}}{\partial y_{NH_3,s}} + \frac{1}{y_{NH_3,s}} - \frac{K_{inh}}{(1+K_{inh}y_{NH_3,s})}\right)\end{aligned} \tag{7}$$

$$\Rightarrow \quad \boxed{o_{NH_3} = 2 + 2\frac{y_{NH_3,s}}{y_{NO,s}}\frac{\partial y_{NO,s}}{\partial y_{NH_3,s}} - \frac{y_{NH_3,s}\left(k_{Ads} + \frac{\partial(k_{Des1}+k_{Des2})}{\partial y_{NH_3,s}} + k_{sscr1}y_{O_2}^{0.32}\frac{\partial y_{NO,s}}{\partial y_{NH_3,s}}\right)}{k_{Ads}y_{NH_3,s} + (k_{Des1}+k_{Des2}) + k_{sscr1}y_{NO,s}y_{O_2}^{0.32}} - \frac{K_{inh}y_{NH_3,s}}{(1+K_{inh}y_{NH_3,s})}} \tag{8}$$

5.2 NH_3 Coverage as a Function of NH_3 Surface Mole Fraction

The model estimated mean NH_3 coverage as a function of the NH_3 surface mole fraction is shown in Figure S4. A linear relationship is observed below an ANR of 0.7, as expected for Langmuir-type adsorption isotherms at low partial pressures.

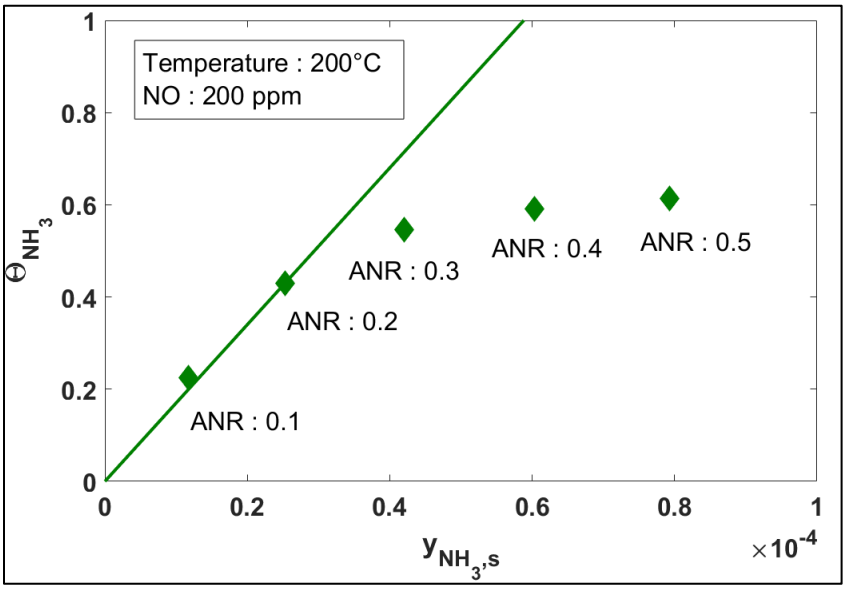

Figure S4. Mean NH_3 surface coverage as a function of NH_3 surface mole fraction. Green diamonds represent model results from ANR sweep at 200°C and solid line represents a linear regression fit

5.3 ANR Sweep Repeatability

ANR sweep experiments were conducted at 200°C to identify the SCR reaction order with NH_3. Each ANR point was repeated three times to establish repeatability, and the results are summarized in Table S3. In general, NO_x conversion and NH_3 storage values were repeatable at all ANRs included in the test, leading to minor deviations in estimated turnover rates and mean NH_3 surface coverages. Turnover rates (TORs) were calculated by normalizing the NO_x consumption rate with the total reducible Cu sites quantified from NO + NH_3 titration experiments.

Table S3

ANR Sweep Test Results at 200°C

NO_x Feed (ppm)	ANR	NH_3 Feed (ppm)	NH_3 Conversion (%)	NO_x Conversion (%)	NH_3 Storage (g/L)	Mean NH_3 Coverage	ln(Mean NH_3 Coverage)	NO_x Flow (mol/s)	TOR (mol_{NO}/mol_{Cu}-s)	ln(TOR)
199.89	0.33	66.37	99.42	33.92	0.71	0.25	-1.40	8.53E-08	1.04E-03	-6.87
201.38	0.33	66.82	99.35	33.17	0.70	0.24	-0.35	8.59E-08	1.02E-03	-6.88
202.80	0.33	67.07	99.50	33.66	0.71	0.24	-0.34	8.65E-08	1.05E-03	-6.86
200.85	0.28	56.26	99.35	28.52	0.62	0.21	-0.48	8.57E-08	8.79E-04	-7.04
201.70	0.28	56.43	99.31	28.78	0.63	0.22	-0.46	8.61E-08	8.90E-04	-7.02
202.78	0.28	56.62	99.34	29.14	0.62	0.21	-0.48	8.65E-08	9.06E-04	-7.01
201.76	0.23	45.60	99.33	23.25	0.51	0.17	-0.68	8.61E-08	7.20E-04	-7.24
202.07	0.23	45.96	99.24	23.44	0.50	0.17	-0.69	8.62E-08	7.27E-04	-7.23
202.75	0.23	46.10	99.26	23.26	0.50	0.17	-0.69	8.65E-08	7.24E-04	-7.23
201.63	0.17	35.14	99.20	18.24	0.43	0.15	-0.83	8.60E-08	5.64E-04	-7.48
202.47	0.17	35.29	98.96	18.34	0.40	0.14	-0.92	8.64E-08	5.70E-04	-7.47
202.51	0.17	35.25	99.07	18.10	0.42	0.14	-0.87	8.64E-08	5.62E-04	-7.48
200.70	0.12	24.53	98.90	12.63	0.30	0.10	-1.21	8.56E-08	3.89E-04	-7.85
202.16	0.12	24.54	98.81	12.59	0.32	0.11	-1.15	8.63E-08	3.90E-04	-7.85
202.55	0.12	24.81	98.90	12.71	0.32	0.11	-1.14	8.64E-08	3.95E-04	-7.84

References

[1] Daya R, Joshi SY, Luo J, Dadi RK, Currier NW, Yezerets A. On kinetic modeling of change in active sites upon hydrothermal aging of Cu-SSZ-13. Applied Catalysis B: Environmental. 2020 Apr 1;263:118368.

[2] Villamaina R, Liu S, Nova I, Tronconi E, Ruggeri MP, Collier J, York A, Thompsett D. Speciation of Cu cations in Cu-CHA catalysts for NH3-SCR: effects of SiO2/AlO3 ratio and Cu-loading investigated by transient response methods. ACS Catalysis. 2019 Aug 20;9(10):8916-27.

[3] Luo J, Gao F, Kamasamudram K, Currier N, Peden CH, Yezerets A. New insights into Cu/SSZ-13 SCR catalyst acidity. Part I: Nature of acidic sites probed by NH3 titration. Journal of Catalysis. 2017 Apr 1;348:291-9.

[4] Paolucci C, Parekh AA, Khurana I, Di Iorio JR, Li H, Albarracin Caballero JD, Shih AJ, Anggara T, Delgass WN, Miller JT, Ribeiro FH. Catalysis in a cage: condition-dependent speciation and dynamics of exchanged Cu cations in SSZ-13 zeolites. Journal of the American Chemical Society. 2016 May 11;138(18):6028-48.

[5] Borfecchia E, Negri C, Lomachenko KA, Lamberti C, Janssens TV, Berlier G. Temperature-dependent dynamics of NH 3-derived Cu species in the Cu-CHA SCR catalyst. Reaction Chemistry & Engineering. 2019;4(6):1067-80.

[6] Daya, R., Trandal, D., Dadi, R. K., Tang, Y., Li, H., Joshi , S.Y., Luo, J., Kumar, A., & Yezerets, A. (2021). Kinetics and thermodynamics of NH_3 solvation on Z_2Cu, ZCuOH and ZCu sites in Cu-SSZ-13 – Implications for hydrothermal aging. *Applied Catalysis B*, submitted.

[7] Paolucci C, Di Iorio JR, Ribeiro FH, Gounder R, Schneider WF. Catalysis science of NOx selective catalytic reduction with ammonia over Cu-SSZ-13 and Cu-SAPO-34. Advances in Catalysis. 2016 Jan 1;59:1-07.

[8] Gao F, Peden CH. Recent progress in atomic-level understanding of Cu/SSZ-13 selective catalytic reduction catalysts. Catalysts. 2018 Apr;8(4):140.